

## Numerical Assessment of Wake Dynamics and Vortex Shedding behind an Array of Equilateral Triangular Cylinders

S.T.W.Kuruneru<sup>1</sup>, E.Sauret<sup>1</sup>, S.C. Saha<sup>1</sup> and Y.T. Gu<sup>1</sup>

<sup>1</sup>School of Chemistry, Physics & Mechanical Engineering, Queensland University of Technology, Brisbane, Queensland, 4011, Australia

### Abstract

A numerical model is employed to examine the wake dynamics behind two equilateral triangular cylinders. Two different configurations are considered—two tandem triangular cylinders and two side-by-side triangular cylinders. A line integral convolution visualization technique is used to study the shed vortices. Results show that the wake topology between the gaps of triangles is dependent on the Reynolds number and centre-to-centre distance. Additionally, correlations between the Reynolds number and Strouhal number at various centre-to-centre distances are obtained.

### Introduction

The dynamical complexity of vortex shedding has attracted considerable interest among engineers and segments of the scientific community. The study of vortex shedding in the vicinity of bluff bodies is of crucial importance in engineering applications such as civil structures and heat exchangers. For instance, a negligible difference between the vortex shedding frequency and resonant frequency of the structure can compromise the structural integrity of an object such as refinery stacks or heat exchanger tube bundles [9]. Although many published studies have investigated Karman streets past circular cylinders, there is diminutive information on laminar vortex shedding past noncircular cylinders such as equilateral triangles. Moreover, the existing literature is devoid of numerical analysis pertaining to multiple triangles arranged in various orientations. Interestingly, the struts of a porous metal foam heat exchanger are triangular [1]. Metal foams are highly porous materials that exhibit superior thermo-physical properties such as low weight, high strength, and high gas permeability, to name a few [4]. The stochastic orientation of these foams coupled with its high surface area to volume ratio greatly induce turbulence, thereby increasing fluid tortuosity and heat transfer performance. Although there exists a myriad of fluid mechanics studies pertaining to metal foams immersed in Newtonian fluids, studies on vortex shedding behind triangles arranged in various configurations is incomplete.

The vortex shedding frequency, mean drag and lift forces, and the wake and proximity interference regimes in the flow behind non-circular cylinders or circular cylinders is dissimilar. These entities are largely dependent on the superficial fluid velocity, and the longitudinal pitch ratio or streamwise separation (distance between the two adjacent cylinders). For instance, Carmo *et al.* [2] used Floquet stability analysis and direct numerical simulation (DNS) to investigate the symmetries and periodicity of three different shedding modes that occur in the wake transition in circular cylinders in staggered arrangements. The modes are present in the wake transition in both single cylinder and staggered arrangement whilst onset of one of the shedding modes depends on the transverse pitch ratio. Zhu [11] used immersed boundary method (IBM) to study the influence of several parameters such as the Reynolds number and

dimensionless fibre length on vortex shedding around a flexible fibre tethered at its centre point. It is found that both the vortex shedding frequency and critical Reynolds number increase linearly as dimensionless fibre length increases. Rao *et al.* [6] elucidated the differences between the wake dynamics of unbounded fluid flow past circular cylinders arranged in tandem and circular cylinders arranged in tandem in close proximity to a rigid wall. At low Reynolds numbers, the cylindrical wakes oscillate at identical frequencies, whereas a *period doubling* is observed at higher Reynolds numbers. However, these studies are restricted to low Reynolds number ( $Re < 300$ ) fluid flow behind circular cylinders. Zhang and Zhou [10] studied vortex shedding patterns and wake topology by varying the distance between three side-by-side circular cylinders. At equal spacing, one wide wake is formed behind the central cylinder, and a single vortex street is formed further downstream. However, at unequal spacing, a narrow wake is formed behind the central cylinder which disappears at a particular streamwise distance resulting in the formation of one asymmetrical vortex street. Staggered arrays of short circular cylinders (*i.e.* pin-fins) immersed in high Reynolds number flows were dominated by periodic vortex shedding [5]. A decrease in the cylinder spacing resulted in the confinement of the near wake length scales thereby increasing the Strouhal number. The Strouhal number ( $St$ ) and Nusselt number ( $Nu$ ), based on a single equilateral triangle immersed in an incompressible fluid, increases monotonically with increasing Reynolds number. The average Nusselt number is shown to be 15 % higher in the case of the triangle obstruction than the square cylinder [8]. However, vortex streets is not considered as the study deals with  $Re < 80$ . The orientation of a triangular cylinder facing the incoming air stream plays a role in the structure of vortices [9]. For a vertex facing the flow, at  $4.16 \leq Re \leq 38.03$ , stable standing counter rotating vortices are formed. However, stable symmetric vortices is realized at  $10 \leq Re \leq 34.7$  if the base of the triangle faces the streamwise flow.

A study based on laminar forced convection fluid flow past a triangular cylinder confined in a channel has shown that the RMS of lift coefficient increases with blockage ratio (*i.e.* ratio of cylinder length to height of channel) and Reynolds number [3]. Secondly, the presence of the channel walls resulted in the delay of the wake transition and first Hopf bifurcation. However, these studies are based on single triangular cylinder only. The flow topology between the gaps of triangular cylinders at various Reynolds numbers and centre-to-centre distances remain elusive. The aim of this work is to examine wake dynamics and vortex streets behind multiple equilateral triangular cylinders.

### Numerical Method and Computational Domain

The motion of an incompressible isothermal fluid with constant fluid properties is governed by the Navier-Stokes equations which is expressed in normalised form as:

$$\frac{\partial u_j}{\partial t} + \frac{\partial(u_j u_k)}{\partial x_k} = -\frac{\partial p}{\partial x_j} + \frac{1}{\text{Re}} \frac{\partial^2 u_j}{\partial x_k \partial x_k}, \quad (1)$$

$$\frac{\partial u_j}{\partial x_j} = 0,$$

where  $\text{Re} (\equiv U_\infty b / \nu_f)$  is based on the free stream velocity  $U_\infty$ , equilateral triangle side length,  $b$ , and fluid kinematic viscosity  $\nu_f$ . In this study, the carrier fluid consists of isothermal gas (air) with kinematic viscosity  $\nu_f$ . The numerical simulation evolves equation (1) using finite volume method (FVM) which is executed in OpenFOAM, an open-source CFD program. The boundary conditions for fluid flow past unconfined multiple cylinders is shown in Table 1. The numerical investigation is performed at two Reynolds numbers of 200 ( $U_\infty = 0.05878$  m/s) and 500 ( $U_\infty = 0.1176$  m/s). To prevent numerical oscillations, the time step is set at 0.0001 s and the simulation is run to 1.00 s based on the Courant-Friedrichs-Lewy (CFL) criteria. The numerical simulation is executed until the residual convergence criteria is achieved which is  $10^{-6}$  and  $10^{-5}$  for the pressure and velocity respectively. A generalized geometric-algebraic multi-grid (GAMG) solver and a Gauss-Seidel smoother is deployed to obtain discretised pressure equations whilst a smoother symmetric Gauss-Seidel (sGS) is used to discretise the velocity equations.

	Velocity $u$	Pressure $p$
<b>Inlet</b>	uniform	zero gradient
<b>Outlet</b>	zero gradient	0
<b>Top &amp; Bottom</b>	slip	zero gradient
<b>Cylinder</b>	no-slip	zero gradient

Table 1. Summary of boundary conditions.

An implicit first-order Euler scheme for discretising the time derivatives and a second-order Gauss linear upwind scheme is used to discretise the convection-diffusion terms of the momentum equations. The computational cost becomes prohibitively expensive with increasing Reynolds number and mesh size. Therefore, in this study, a merged SIMPLE-PISO (*i.e.* PIMPLE) numerical algorithm is used to achieve faster convergence. To ensure a stable pressure-momentum coupling, the PIMPLE loop is controlled by assigning two correctors and twenty non-outer correctors. The morphological description of the computation domain and boundary conditions is shown in figure 1. The equilateral side length of the triangular cylinder is 0.025 m. The dimension of the computation domain is 0.9 m ( $H$ )  $\times$  0.80 ( $W$ ). A close-up of the mesh used in this study is illustrated in figure 2. The computation domain and mesh is created in ANSYS Fluent, afterwards the mesh is exported to OpenFOAM to perform the numerical simulations. The mesh consists of structured grids in general coordinates based on quadrilateral elements. The mesh is refined around the triangle by using the edge sizing mesh control. Numerical analysis of the flow topology of the two cases is examined at various centre-to-centre distances,  $W_c$  (figure 1 and figure 2). The effects of varying the upstream streamwise distance ( $W_u$ ) and upstream height ( $H_u$ ) on the mean drag coefficient was numerically examined, and it was found that the mean drag coefficient  $C_d$  becomes independent of the upstream and downstream distance at 0.20 m and 0.40 m respectively. An artificial blockage ratio  $\beta (\equiv b/H)$  is assigned a value of 1/32 to ensure that such blockage ratio has negligible effect on the flow topology around the vicinity of the triangular obstruction walls [7]. Several meshes were constructed to conduct a grid independence study to assess the mesh dependence on the pressure drop and Strouhal number ( $St$ ). It is found that mesh independence is achieved at 121, 093 nodes and 123,750 nodes for case 1 and case 2 respectively.

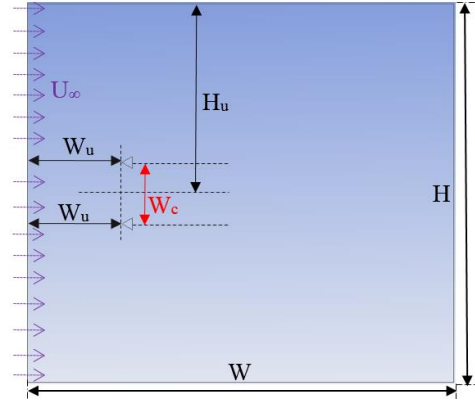


Figure 1. Computation domain of fluid flow past equilateral triangular cylinders arranged in a side-by-side configuration (Case 1).

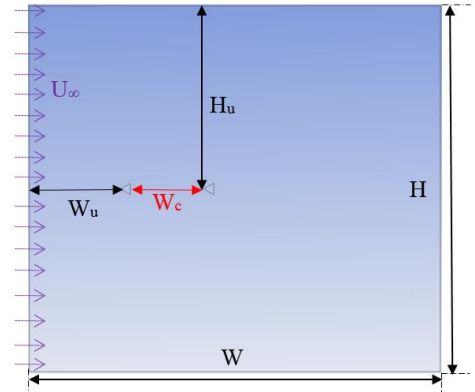


Figure 2. Computation domain of fluid flow past equilateral triangular cylinders arranged in a tandem configuration (Case 2).

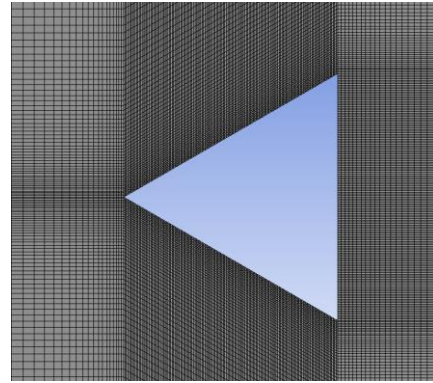


Figure 3. Magnified view of computational grid for blockage ratio of 1/32

### Numerical Model Validation

A validation assessment is performed based on flow past a single triangular cylinder for three different Reynolds numbers. The numerical study of Zeitoun et al. [9] is used as a benchmark to compare the drag coefficients in the present study. The computation domain and boundary conditions for the validation study is similar to Zeitoun et al. [9]. According to Table 2, the present numerical results is within an acceptable 8–12 % of the values obtained in the literature, thus lending credence to the present numerical solution procedure. Unfortunately, there exists no experimental results for the conditions presented herein.

Re	27.76	69.40	180.00
<b>Present study (<math>C_d</math>)</b>	2.006	1.742	2.184
<b>Zeitoun et al. [9] (<math>C_d</math>)</b>	1.817	1.576	1.940

Table 2. Comparison of results with existing literature.

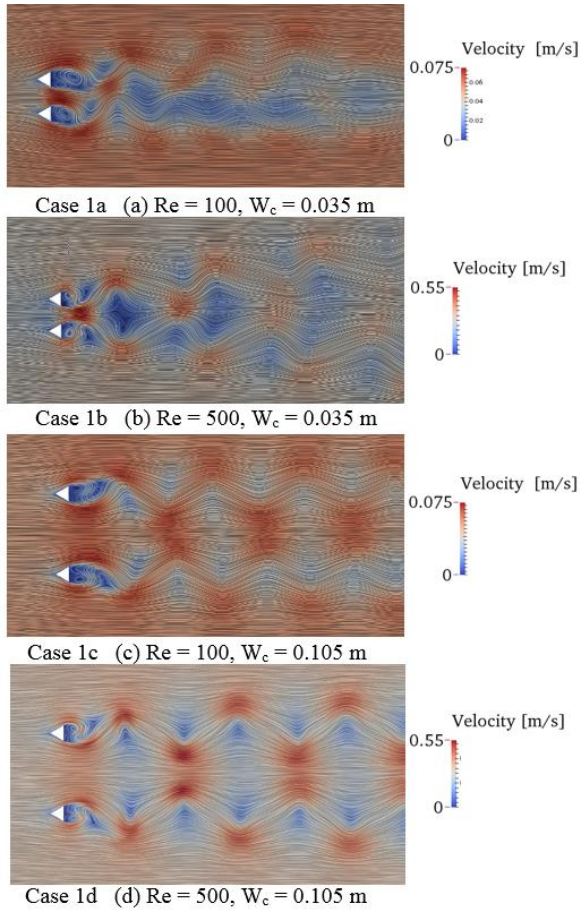


Figure 4. Contour plot for cylinders arranged in side-by-side (Case 1).

## Results and Discussion

The velocity contours illustrating wake dynamics and vortex shedding of the two cases is illustrated in figure 4 and figure 5. A line integral convolution (LIC) visualization technique is used to conscientiously visualize fluid wake and vortices.

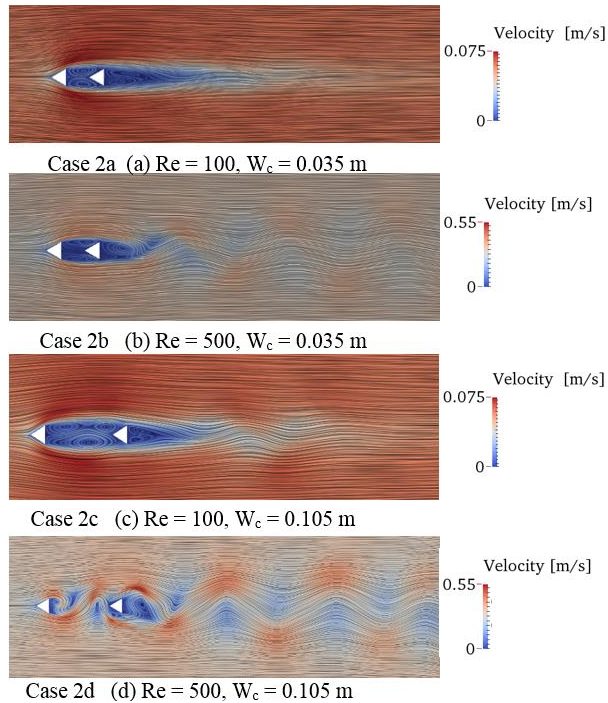


Figure 5. Contour plot for cylinders arranged in tandem (Case 2).

The onset of flow separation commences once the fluid nears the separation point at the tip of the triangular cylinder (facing the streamwise direction). Case 1 exhibits traits of proximity interference where the fluid wake of one triangle does not partially or completely submerge the other triangle. It is noted that at  $W_c = 0.035 \text{ m}$ , the fluid wake located downstream of the top and bottom cylinder superimposes to form a wake with a larger surface area (blue contour) as shown in case 1a and case 1b. The flow is sensibly biased towards the bottom cylinder as shown in case 1a. This proximity interference effect, which is the dominant flow profile in Case 1, ultimately leads to flow patterns being locked in an anti-phase vortex synchronization mode downstream of the cylinder pair. Case 1a behaves as a single bluff body where a single Karman vortex street is formed, whereas the other three cases depicted in cases 1b, 1c, and 1d all behave as independent isolated bluff bodies. According to figure 4 (*i.e.* case 1), asymmetric eddies are formed adjacent to the surface behind both triangles. The vortices behind side-by-side triangles from both triangles start to intermingle at a critical centre-to-centre distance  $W_{cc}$  of  $0.070 \text{ m}$ .

The cylinders arranged in tandem configuration (figure 5) showed stark differences in the flow characteristics. The fluid encapsulates the entire cylinder, and depending on the Reynolds number and centre-to-centre separation distance, shed vortices are generated. A key difference is that the tandem configurations exhibit wake interference flow characteristics. Moreover, unlike the side-by-side triangles, the tandem triangles are completely shielded from the oncoming upstream flow by the frontal triangle. A single vortex street structure is omnipresent in cases 2b, 2c, and 2d. Interestingly, case 2d shows an additional vortex street located in the gap between the two triangles which is accompanied by a larger vortex street in the downstream cylinder. Cases 2a, 2b, and 2c show characteristics of single bluff-body behaviour or *extended-body regime*; whereas case 2d shows shear layer reattachment behaviour or in other words *reattachment regime* where vortices are formed in the gap and the shear layer from the surface of the upstream triangle reattaches onto the downstream triangle. The wake in case 2d is characterized by double shed vortices. The vortices become considerably elongated at  $Re = 500$  irrespective of the centre-to-centre distance  $W_c$  compared to  $Re = 100$ . The shed Karman vortices in the reattachment regime amplify more rapidly compared to the extended-body regime. Only case 2a is sensibly devoid of any vortex streets past the downstream cylinder. The two tandem cylinder arrangement shows greater propensity to inhibit or impair the vortex shedding process compared to the two side-by-side cylinder arrangement.

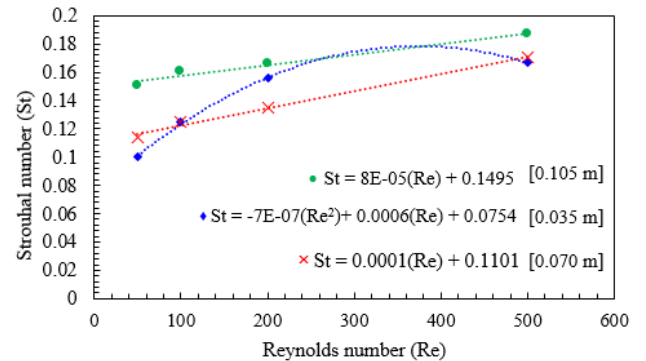


Figure 6. Strouhal number as a function of Reynolds number for triangles arranged in tandem computed at  $Re=50,100,200,500$ ;  $\times$ ,  $W_c = 0.070 \text{ m}$ ;  $\bullet$ ,  $W_c = 0.105 \text{ m}$ ;  $\blacklozenge$ ,  $W_c = 0.035 \text{ m}$ .

Irrespective of Reynolds numbers, both cases 2a and 2b show symmetric eddies between the two triangular cylinders and

asymmetric eddies behind the downstream (second) cylinder. It is noted that the eddies become elongated (*i.e.* elliptical) as Reynolds number increases (case 2b). Interestingly, asymmetric eddies are observed in cases 2c between the two cylinders whereas symmetric eddies is realized behind the downstream cylinder. However, an increase in the Reynolds number (from case 2c to case 2d) shows shear layers being separated from the upstream cylinder which engulfs the downstream cylinder to form a vortex street.

The Strouhal number  $St$  ( $\equiv fb/U_\infty$ ), which is a function of the dominant frequency of vortex shedding  $f$ , triangular cylinder side length  $b$ , and flow velocity  $U_\infty$ , is plotted against Reynolds number and shown in figure 6 and figure 7. The dominant frequency  $f$ , shown in figure 8 and figure 9, is obtained by evaluating the fast Fourier transform (FFT) of the lift coefficient of a particular case study. The two peaks (dotted circles) in cases 2b and 2d may be ascribed to the fluid shear layer reattaching the downstream cylinder. At 0.035 m and 0.070 m, a linear relationship between the Strouhal number and Reynolds number is obtained by plotting a line of best fit. It is interesting to note that for the side-by-side configuration, a second order polynomial fitting is discernible at the highest centre-to-centre distance  $W_c$ —0.105 m (figure 7); whereas, the tandem configuration exhibited this quadratic relationship at the lowest  $W_c$  value at 0.035 (figure 6).

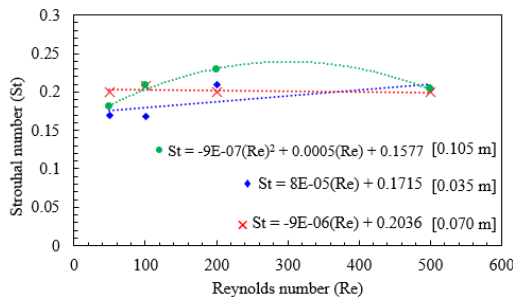


Figure 7. Strouhal number as a function of Reynolds number for cylinders arranged side-by-side computed at  $Re=50,100,200,500$ ;  $\times$ ,  $W_c = 0.070$  m;  $\bullet$ ,  $W_c = 0.105$  m;  $\blacklozenge$ ,  $W_c = 0.035$  m.

The Strouhal number for the tandem cases with  $W_c = 0.1070$  m and 0.105 m increases monotonically with increasing value of the Reynolds number for the tandem configuration as shown in figure 6. According to figure 7, the Strouhal number for two side-by-side cylinder at 0.070 m is almost independent of the Reynolds number with a maximum Strouhal difference at 5.3 %. The Strouhal number for tandem triangle is higher than side-by-side cylinder irrespective of the  $Re$  and  $W_c$ .

## Conclusions

A numerical model is developed in OpenFOAM to examine the wake dynamics and shed vortices behind equilateral triangles. Variation in Reynolds number and centre-to-centre distances has a substantial influence on the flow topology. Superimposition of fluid wake is discerned in side-by-side triangles at a specific  $W_c$  value. Extended body regime is the dominant flow characteristic in tandem triangles. Strouhal number and Reynolds number is obtained for various  $W_c$  values in which the majority of cases show a linear relationship.

## References

[1] Bock, J. & Jacobi, A., Geometric classification of open-cell metal foams using X-ray micro-computed tomography, *Materials Characterization*, **75**, 2013, 35-43.

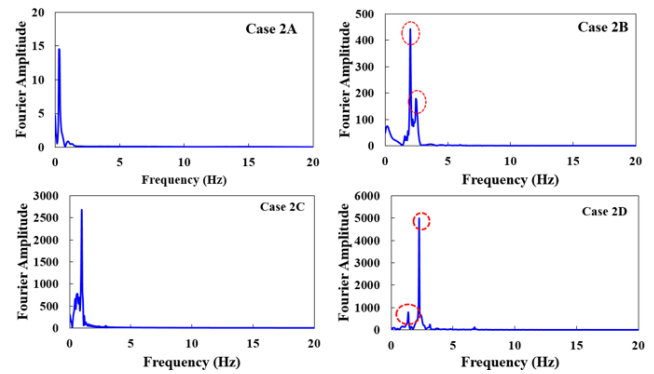


Figure 8. Fourier amplitude of two tandem cylinders.

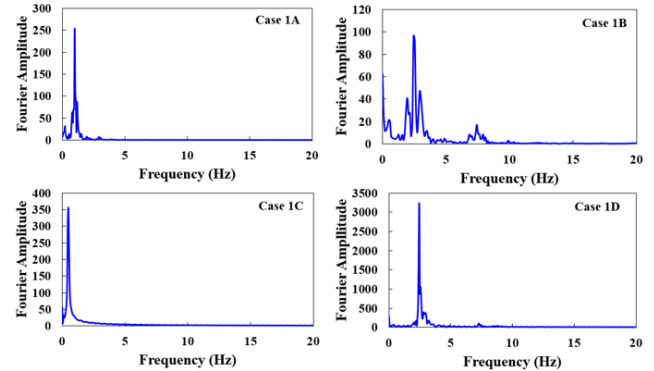


Figure 9. Fourier amplitude of two side-by-side cylinders.

[2] Carmo, B. S., Sherwin, S. J., Bearman, P. W. & Willden, R. H. J., Wake transition in the flow around two circular cylinders in staggered arrangements, *J. Fluid Mech.*, **597**, 2008, 1-29.

[3] De, A. K. & Dalal, A., Numerical study of laminar forced convection fluid flow and heat transfer from a triangular cylinder placed in a channel, *J. Heat T.*, **129**, 2007, 646-656.

[4] Han, X., Wang, Q., Park, Y., T'Joel, C., Sommers, A. & Jacobi, A., A review of metal foam and metal matrix composites for heat exchangers and heat sinks. *Heat Transfer Engineering*, **33**, 2008, 991-1009.

[5] Ostanek, J. K. & Thole, K. A., Wake development in staggered short cylinder arrays within a channel. *Exp. Fluids*, **53**, 2012, 673-697.

[6] Rao, A., Thompson, M. C., Leweke, T. & Hourigan, K. Dynamics and stability of the wake behind tandem cylinders sliding along a wall. *J. Fluid Mech.*, **722**, 2013, 291-316.

[7] Sohankar, A., Norberg, C. & Davidson, L., Low-Reynolds-number flow around a square cylinder at incidence: Study of blockage, onset of vortex shedding and outlet boundary condition. *Int. J. for Num. M. Fluids*, **26**, 1998, 39-56.

[8] Srikanth, S., Dhiman, A. K. & Bijjam, S., Confined flow and heat transfer across a triangular cylinder in a channel. *Int. J. of Thermal Sciences*, **49**, 2010, 2191-2200.

[9] Zeitoun, O., Ali, M. & Nuhait, A., Convective heat transfer around a triangular cylinder in an air cross flow. *Int. J. of Thermal Sciences*, **50**, 2011, 1685-1697.

[10] Zhang, H. J. & Zhou, Y., Effect of unequal cylinder spacing on vortex streets behind three side-by-side cylinders, *Physics of Fluids*, **13**, 2001, 3675-3686.

[11] Zhu, L., Viscous flow past a flexible fibre tethered at its centre point: Vortex shedding. *J. Fluid Mech.*, **587**, 2007, 217-23.